iScience

CellPress
OPEN ACCESS

Article

Different macaque brain network remodeling after spinal cord injury and NT3 treatment

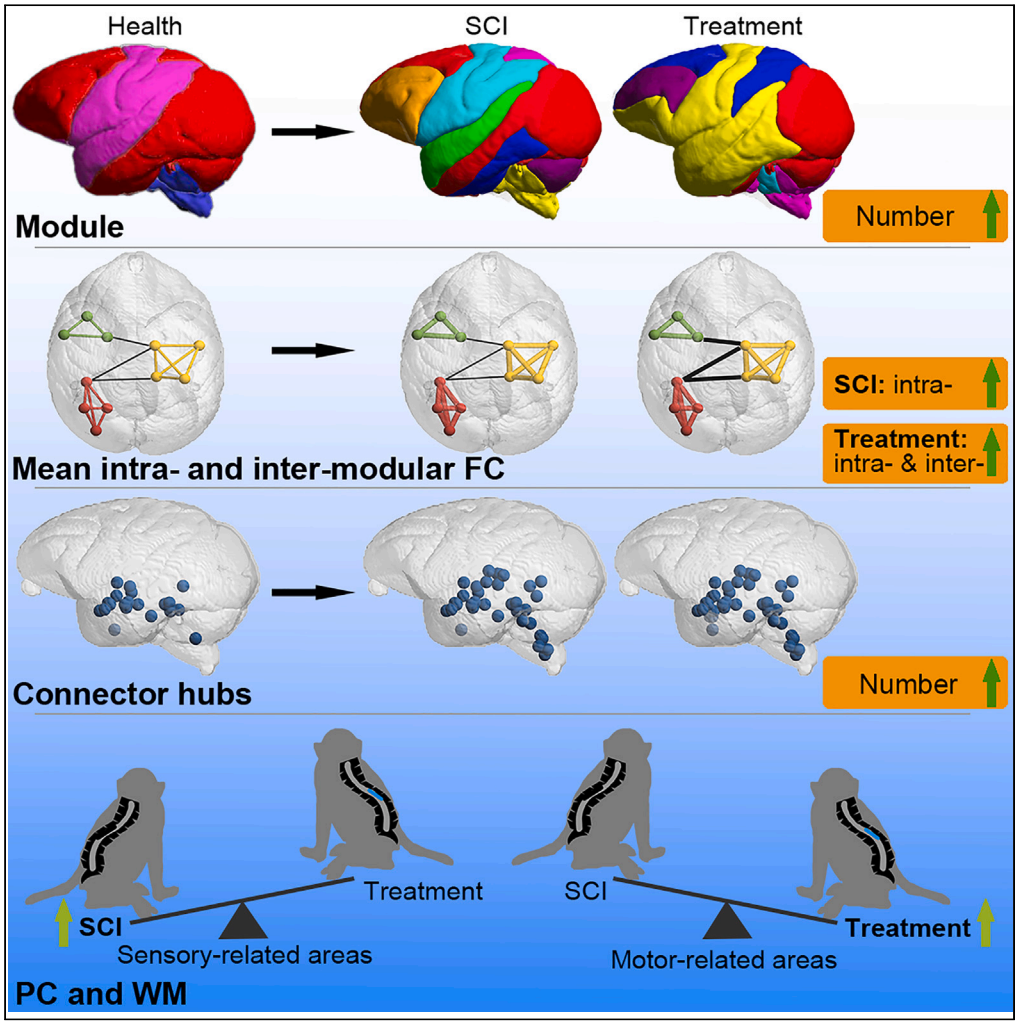

Ting Feng, Can Zhao, Jia-Sheng Rao, ..., Zuxiang Liu, Zhao-Yang Yang, Xiao-Guang Li

raojschina@126.com (J.-S.R.)
zxliu@ibp.ac.cn (Z.L.)
wack_lily@163.com (Z.-Y.Y.)
lxgchina@sina.com (X.-G.L.)

Highlights

We explored the topological properties of brain networks after SCI and NT3 therapy

SCI and NT3 treatment increase the number of modules and connector hubs

SCI increases within-module degree & participation coefficient in sensory areas

Therapy increases within-module degree & participation coefficient in motor areas

Feng et al., iScience 26, 106784
June 16, 2023
https://doi.org/10.1016/j.isci.2023.106784

iScience

CellPress
OPEN ACCESS

Article

Different macaque brain network remodeling after spinal cord injury and NT3 treatment

Ting Feng,[1] Can Zhao,[2] Jia-Sheng Rao,[1,7,*] Xiao-Jun Guo,[1] Shu-Sheng Bao,[1] Le-Wei He,[1] Wen Zhao,[3] Zuxiang Liu,[4,5,6,*] Zhao-Yang Yang,[3,*] and Xiao-Guang Li[1,*]

SUMMARY

Graph theory-based analysis describes the brain as a complex network. Only a few studies have examined modular composition and functional connectivity (FC) between modules in patients with spinal cord injury (SCI). Little is known about the longitudinal changes in hubs and topological properties at the modular level after SCI and treatment. We analyzed differences in FC and nodal metrics reflecting modular interaction to investigate brain reorganization after SCI-induced compensation and neurotrophin-3 (NT3)–chitosan-induced regeneration. Mean inter-modular FC and participation coefficient of areas related to motor coordination were significantly higher in the treatment animals than in the SCI-only ones at the late stage. The magnocellular part of the red nucleus may reflect the best difference in brain reorganization after SCI and therapy. Treatment can enhance information flows between regions and promote the integration of motor functions to return to normal. These findings may reveal the information processing of disrupted network modules.

INTRODUCTION

Every year, 250,000–500,000 people worldwide suffer from spinal cord injury (SCI), which interrupts the efferent (motor) and afferent (sensory) connections between the cerebral cortex and the spinal cord. SCI can result in motor and sensory dysfunction,[1,2] which severely affects functional independence and quality of life.[3,4] Restoring the motor function of patients with SCI to the greatest extent has always been a hot and difficult issue in clinical research. In the past few decades, many researchers have analyzed various methods to repair SCI, such as cell transplantation,[5–7] neurotrophic drug injection,[8] tissue engineering,[9,10] and biomaterial implantation.[11–14] These treatments promote the recovery of residual structure/function, integration of replacement tissues, and formation of new neurons/fibers in the injured area. The bioactive material (neurotrophin-3 [NT3]–chitosan) previously developed by our group has been shown to trigger the robust activation of endogenous neural stem cells (NSCs) in the injured spinal cord of non-human primates. The bioactive material attracts NSCs to migrate to the injured area through the slow release of NT3 and NSCs, which are differentiated into neurons. Enhanced angiogenesis and reduced inflammatory responses also provide a favorable microenvironment for neurons. These biological effects promote the formation of functional neural networks that rebuild severed connections, leading to the restoration of sensorimotor functions.[14]

The spinal cord is responsible for the transmission and integration of signals to and from the brain. The nervous system undergoes major remodeling after SCI. Brain–spinal cord interactions and dynamic changes in function play a crucial role in the reconfiguration of neurological function, which may have important clinical implications for the treatment of patients with SCI and evaluation of their efficacy. Previous studies mostly focused on the local injury regions of the spinal cord, and there now has been a growing focus on brain research in recent years. The brain is closely related to the structure and function of the spinal cord. Quantifying brain network changes after SCI can further improve the understanding of the mechanisms of brain reorganization induced by SCI and help develop appropriate rehabilitation treatment plans for patients suffering from SCI with motor/sensory dysfunction and neuropathic pain.

Blood-oxygen-level-dependent fMRI technology can be applicable for identifying interactive brain regions during non-task states to detect endogenous brain activity. The detection indicators of non-task state fMRI data after post-processing can reflect the nature of local and whole-brain activity, of which functional

[1]School of Biological Science and Medical Engineering, Beijing Key Laboratory for Biomaterials and Neural Regeneration, Beijing Advanced Innovation Center for Biomedical Engineering, Beihang University, Beijing, PR China

[2]Institute of Rehabilitation Engineering, China Rehabilitation Science Institute, Beijing, PR China

[3]Department of Neurobiology, School of Basic Medical Sciences, Capital Medical University, Beijing, PR China

[4]State Key Laboratory of Brain and Cognitive Science, Institute of Biophysics, Chinese Academy of Sciences, Beijing, PR China

[5]Institute of Artificial Intelligence, Hefei Comprehensive National Science Center, Hefei, PR China

[6]Department of Biology, College of Life Sciences, University of Chinese Academy of Sciences, Beijing, PR China

[7]Lead contact

*Correspondence: raojschina@126.com (J.-S.R.), zxliu@ibp.ac.cn (Z.L.), wack_lily@163.com (Z.-Y.Y.), lxgchina@sina.com (X.-G.L.)

https://doi.org/10.1016/j.isci.2023.106784

connectivity (FC) is the most widely used because it can depict activity consistency across regions. Over the past two decades, an increasing number of clinical studies have employed fMRI technology and subsequent FC calculations to characterize cortical connectivity changes after SCI.[15–20] Most of these studies focused on FC of sensorimotor areas after SCI to explore compensation and functional changes in sensorimotor cortical regions.[21,22]

In addition to studies on compensatory changes in local brain regions, Bullmore et al.[23] proposed a graph-theoretical approach using brain regions as nodes and FC values between brain regions as edges to form a large-scale brain network to analyze the global and local topological properties of networks.[23,24] At present, numerous brain fMRI studies applying a graph-theoretical method have been carried out in neurological diseases such as Alzheimer disease[25,26] and epilepsy.[27] These studies using a graph-theoretical method revealed abnormal functional network states induced by diseases, as well as provided new insights into the diagnosis and new hopes for the treatment of these diseases. As SCI research has advanced, a small number of studies have also begun to focus on abnormalities of whole-brain functional networks using a graph-theoretical approach to explore the heterogeneity of brain network modules in patients with SCI.[28,29] These changes of modules reflect the topological properties of brain networks, modularity, which suggests that the brain network is densely connected within modules and sparsely connected between modules. Topological properties of functional networks (i.e., connectomics)[30,31] must reveal the integration and separation of brain functions after SCI. Hawasli et al.[28] used a graph-theoretical approach to analyze functional networks and found that SCI disrupts the internal connectivity of the default mode network (DMN) and the normal connectivity between the executive control network and somatosensory motor network (SMN) network. Kaushal et al.[29] performed large-scale functional network analysis in patients with complete cervical SCI and found that FC of whole-brain subnetworks in patients with SCI decreased, whereas FC between the sensorimotor cortex and the subnetwork of the cerebellar network increased. Kaushal et al.[32] applied a modular algorithm to perform graph-theoretical analysis of patients with complete SCI. The functional network of patients with SCI was divided into nine modules and the number and composition of nodes in each module differed from those of healthy subjects; the local efficiency of the functional network showed a statistically significant decrease at multiple thresholds. Although these studies have observed disruption of brain modular organization after SCI, injury-induced alterations in modular properties, such as hubs, remain unclear. Hubs play a central role in brain communication and neural integration. They were provincial hubs highly linked within their own modules for specialized functions, and connector hubs linking different modules. In addition, there are no reports of functional brain network changes following regenerative treatment for SCI. Theoretically, reconfigured neural projections can reshape connections between peripheral nerves and brain, so "silent" brain areas are activated and other brain areas closely connected to them are affected. How these pathophysiological changes alter the properties of brain networks remains to be explored in depth.

To explore the effects of SCI and regenerative treatment on the reorganization of functional brain networks and changes in modular properties, we longitudinally investigated changes in the modular topology of the whole brain after SCI and NT3 treatment in rhesus monkeys using a graph-theoretical approach. We hypothesized that SCI animals would exhibit abnormalities in intra- and inter-modular FCs, whereas regenerative treatment animals would alleviate such changes to some extent. In this study, the mean intra- and interhemispheric FCs, intra- and inter-modular FCs, within-module degree (WM), and participation coefficient (PC) were calculated and intergroup differences were analyzed to characterize information exchange patterns within and between different brain modules and understand underlying the functional reorganization mechanism after SCI and NT3 treatment.

RESULTS

Modular reorganization and increased mean intrahemispheric FC after SCI

In this study, 470 cortical and subcortical ROIs (235 brain regions on the left and right sides with reference to the INIA19 rhesus monkey brain atlas) were selected, and 470 × 470 network matrices were constructed using fMRI data under anesthesia state. Every whole-brain network was divided into different modules, and intergroup module differences in rhesus monkeys were analyzed at the healthy period and at 1, 2, 3, 6, and 12 months postoperatively.

The brain network at the healthy period in rhesus monkeys was divided into five modules: default mode network (module 1, red), brainstem structure (module 2, blue), somatosensory motor network and salience

network (module 3, purple), limbic system (module 4, yellow), and cerebellar network (module 5, cyan). Module 1 mainly includes brain regions such as the precuneus, inferior temporal gyrus, posterior cingulate gyrus, and superior frontal gyrus. Module 2 mainly contains the solitary nucleus, spinal trigeminal nucleus, dorsal cochlear nucleus, facial nucleus, and other nuclei related to visceral sensation and somatosensation. Module 3 mainly includes brain areas such as precentral gyrus, postcentral gyrus, and insula. Module 4 mainly has structures such as amygdala, hippocampus, dentate gyrus, and hypothalamus. Module 5 mainly has structures such as fastigial nucleus, dentate nucleus, globose pallidus, and lobule III. The brain functional networks in the SCI-only group at 1, 2, 3, 6, and 12 months postoperatively were divided into 6, 7, 9, 7, and 9 network modules, respectively; meanwhile, 9, 6, 8, 6, and 11 network modules in the treatment group were obtained, respectively (Figure 1A). The SCI-only group and treatment group showed varying degrees of increases in the number of modules at multiple postoperative time points, indicating enhanced functional separation of the entire brain network after SCI and NT3 treatment.

Further analysis about modular separation revealed no significant difference in mean FC strength between the left insula and bilateral somatosensory areas within 2 months postoperatively (early stage) for the SCI-only group and treatment group. The above FC strength was similar to it in the healthy period. At 3–12 months postoperatively (late stage), however, a significant group difference was found in the FC strength ($p = 0.011$). The FC strength in the SCI-only group was significantly lower than that in the treatment group ($p = 0.04972$) and the healthy period ($p = 0.033$), but no difference was noted between the treatment group and the healthy period (Figure 1B). Different from the left hemisphere, no significant difference was found among the three groups for mean FC strength between the insula in the right hemisphere and bilateral somatosensory areas.

The examined results of the right hindlimb's normalized thermal pain threshold (NTPT) corresponding to the left hemisphere showed that the NTPT of SCI-only group was clearly lower than that of the treatment group ($p = 0.017$) and the healthy period ($p = 0.003 \times 10^{-3}$) (Figure S1A). Moreover, a significant positive correlation was also observed for mean FC strength between the left insula as well as bilateral somatosensory areas and the NTPT (SCI-only group: $r = 0.530$, $p = 0.010$; treatment group: $r = 0.506$, $p = 0.012$; Figure S1B).

In the late stage, a significant between-group difference was found in mean intrahemispheric FC strength ($p = 0.020$), and the mean intrahemispheric FC strength in the SCI-only group was significantly higher than that in the healthy period ($p = 0.042$). Thus, functional integration within the cerebral hemispheres occurred in the SCI-only group at the late stage of injury (Figure 2).

Decreased provincial hubs and increased connector hubs

During the healthy period, connector hubs of the brain network were mainly distributed in sensory and motor-related brain areas such as lobule III and mesencephalic nuclei of the trigeminal nerve, whereas provincial hubs were mainly found in brain regions such as medial dorsal nucleus, thalamus, amygdala, hippocampus, and dentate nucleus. Brain regions in the limbic system and higher sensory centers such as thalamus, hippocampus, and amygdala were developed from provincial hubs to connector hubs after SCI. In addition, brain regions in the treatment group that were originally non-hubs, such as the midbrain and inferior colliculus, were developed into connector hubs. By 12 months, the magnocellular part of the red nucleus became connector hubs. In addition, the superior central nucleus, dorsal raphe nucleus, cuneiform nucleus, and parvicellular reticular nucleus in the brainstem gradually became connector hubs in the treatment group to support functional integration of the whole-brain network (Figure 3A). The quantification result of hubs at different time points is shown in Figure 3B, where an increase in connector hubs in the SCI-only group and treatment group can provide additional support for enhanced integration of network functions (Figure 3B).

High mean intra- and inter-modular connectivity after treatment

Longitudinal analysis showed that for the SCI-only group, mean inter-modular connectivity did not vary with the injury time, whereas mean intra-modular connectivity was significantly correlated with the injury time ($p = 0.001$). Both mean intra-modular connectivity ($p = 0.004 \times 10^{-3}$) and mean inter-modular connectivity ($p = 0.003 \times 10^{-1}$) were correlated with time in the treatment group (Figure 4). The comparison between groups showed that the mean inter-modular connectivity in the early stage in both the SCI-only group and treatment group were similar, both of which were not different from the healthy period.

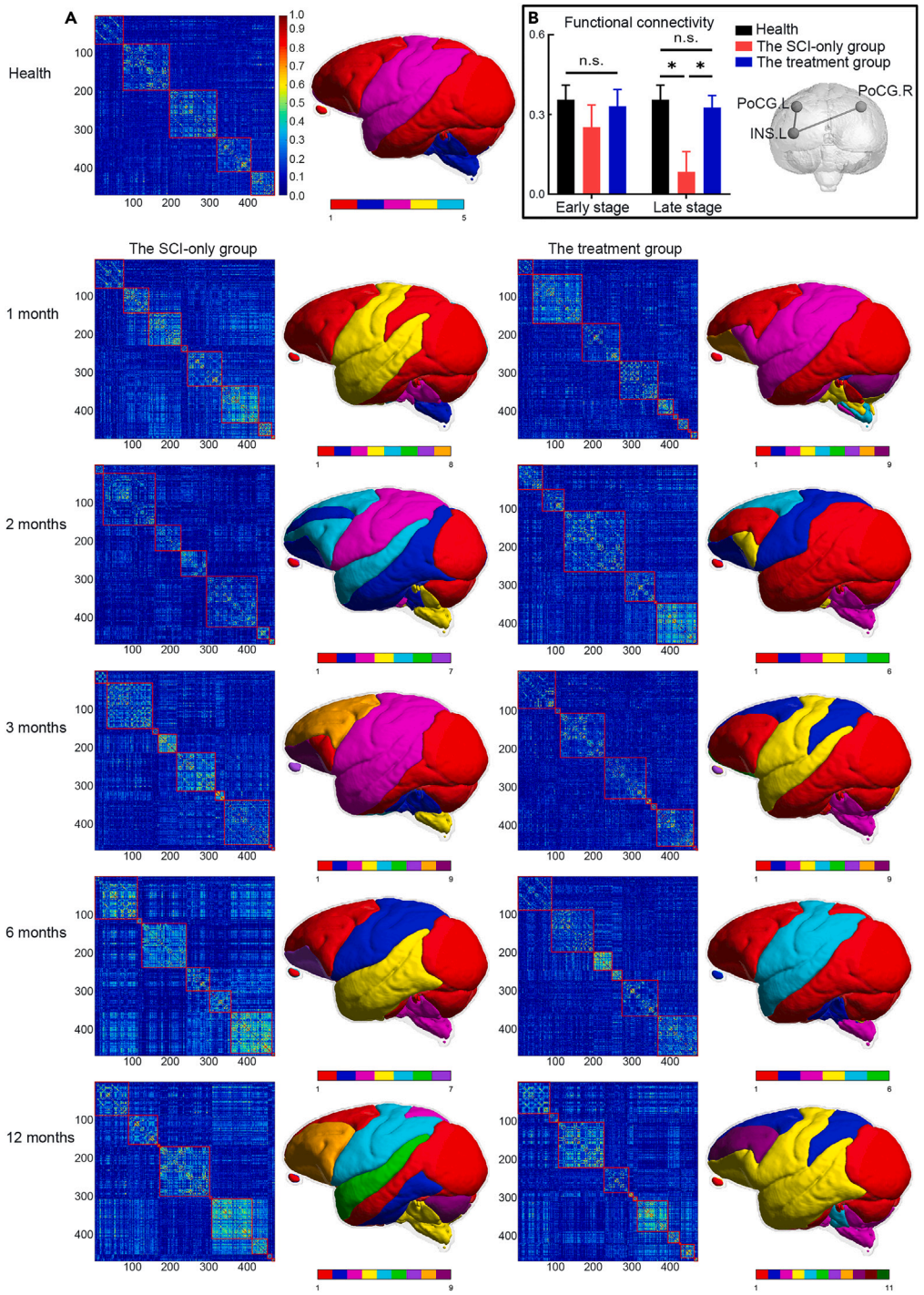

Figure 1. Visualization of group-level functional brain network matrixes constructed from fMRI data under anesthesia state, spatial distribution of brain modules, and between-group differences of averaged FC between the left insula and bilateral somatosensory areas

(A) Left column: Group-level functional connectivity matrix was reorganized by its modular organization with red boxes and expressed as correlations among 470 brain regions. Right column: Modules were identified based on the parcellation of the group in each time point. Different color schemes depict different modular communities.

(B) Between-group differences in the strength of averaged functional connectivity between the left insula and bilateral somatosensory areas in the early- and late-stages after surgery (both post-hocs: LSD). Data are shown as mean values and standard errors. PoCG, postcentral gyrus; INS, insula; *p < 0.05. *n.s.*, none significance.

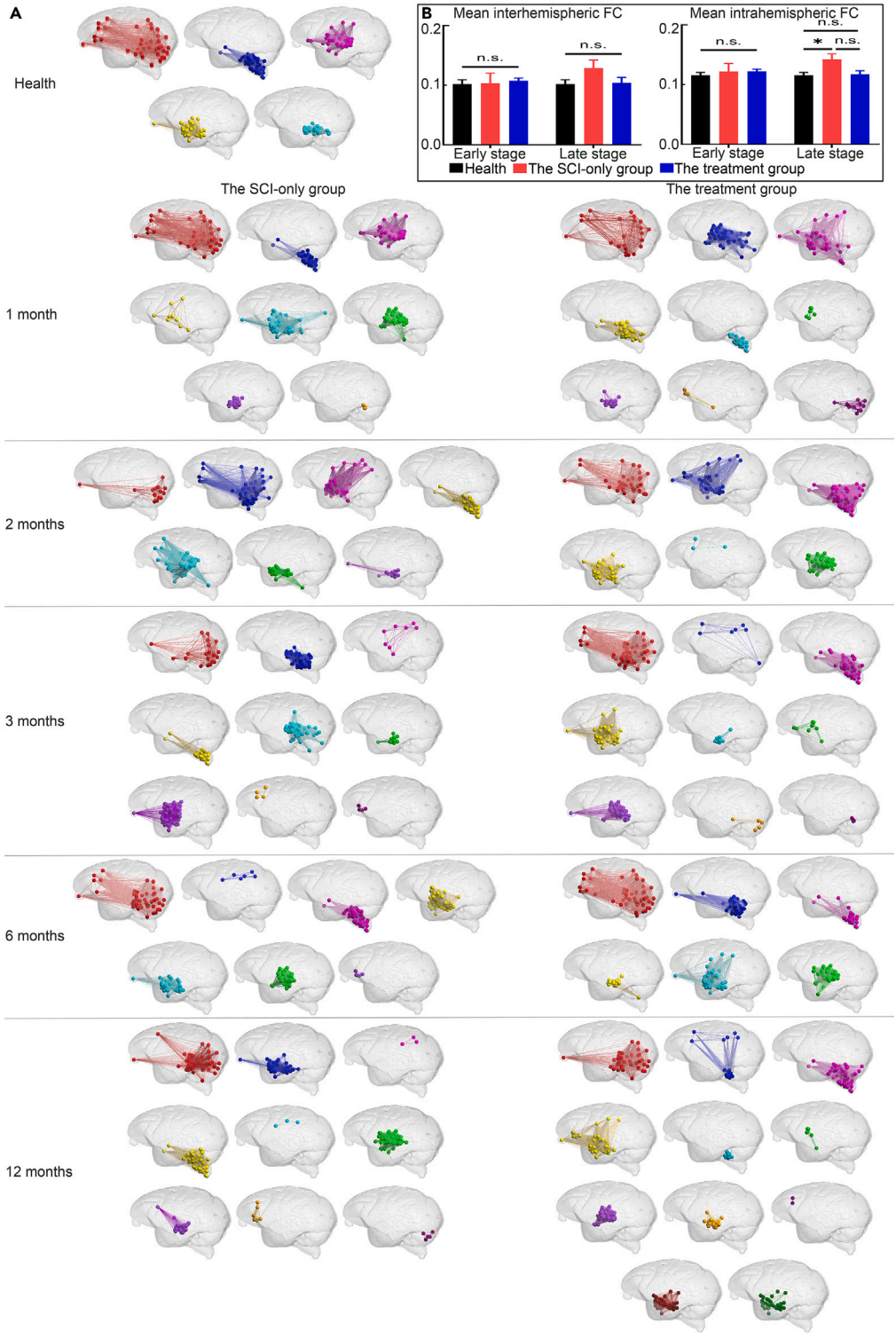

Figure 2. Visualization of module, mean interhemispheric and intrahemispheric connectivity results, and comparison

(A) The brain networks' modular reorganizations were visualized. The nodes represent spatial locations of the brain regions, and the edges represent the connections among the nodes.

(B) Between-group differences in the strength of mean interhemispheric and intrahemispheric functional connectivity among the three groups in the early- and late-stages post-SCI (post-hoc: Games-Howell). Group mean values and standard errors are shown. *$p < 0.05$. *n.s.*, none significance.

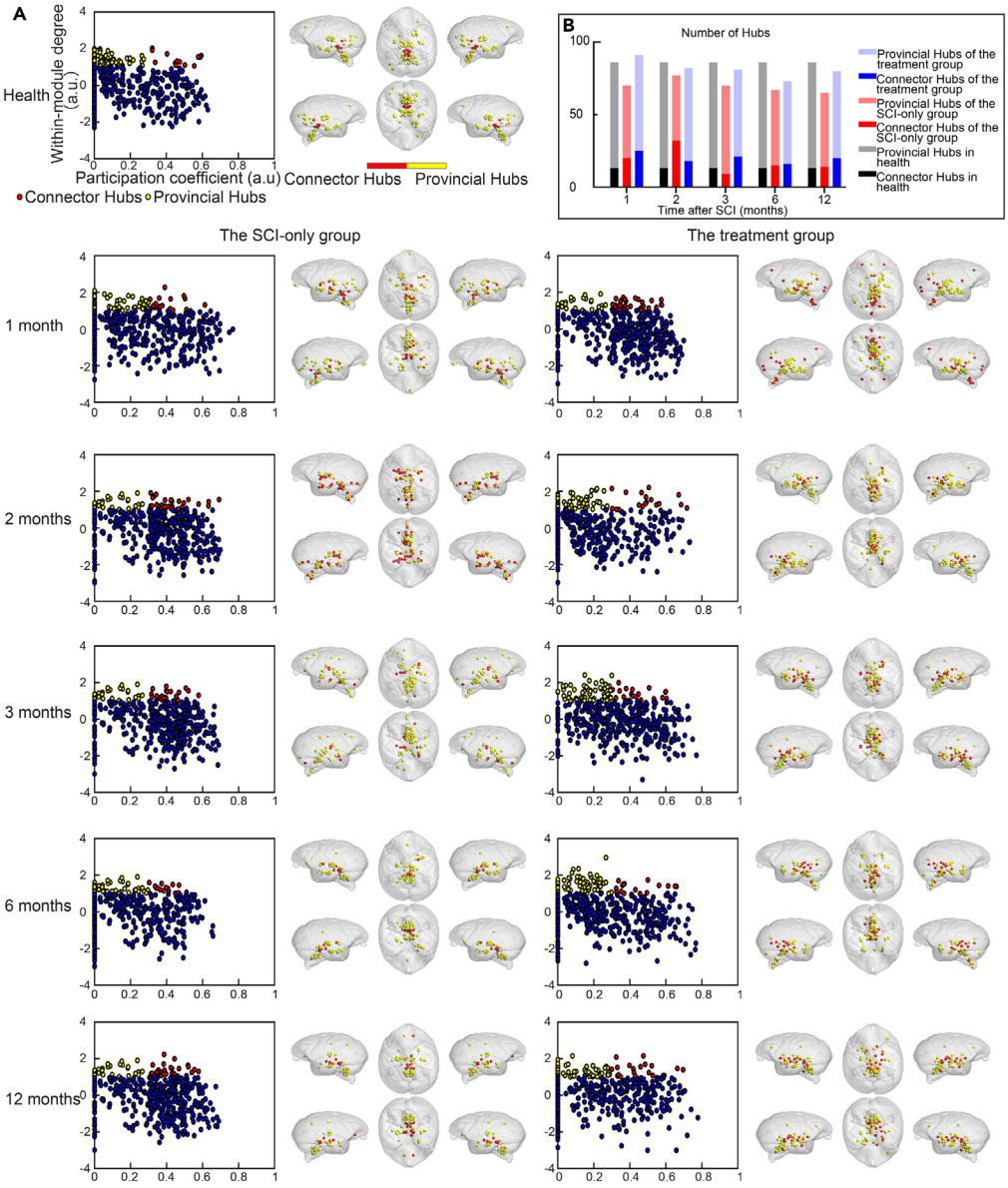

Figure 3. Differences in spatial distribution and the number of two types of hubs

(A) Left column: Network-specific normalized within-module degree and participation coefficient. Right column: Provincial and connector hubs in brain functional networks. Spatial distribution of provincial (yellow) and connector hubs (red) across the three groups.

(B) The number of provincial and connector hubs.

However, in the late stage, the mean inter-modular connectivity in the treatment group was significantly enhanced ($p = 0.002$). Mean intra-modular connectivity was the same in the early and late stages, with the lowest connectivity at the healthy period. Mean intra-modular connectivity in both the SCI-only group and treatment group was significantly higher than that in the healthy period ($p < 0.018$; Figure 4).

Participation coefficient and within-module degree

Node-level analysis revealed a highly complex change mode in brain networks after SCI and NT3 treatment. In the late stage, the SCI-only group showed significantly decreased PC in several brain regions, involving brain regions related to cognitive and motor control such as left precentral gyrus, bilateral subthalamic nuclei, bilateral magnocellular parts of the red nucleus, and right insula (Figure 5; detailed data

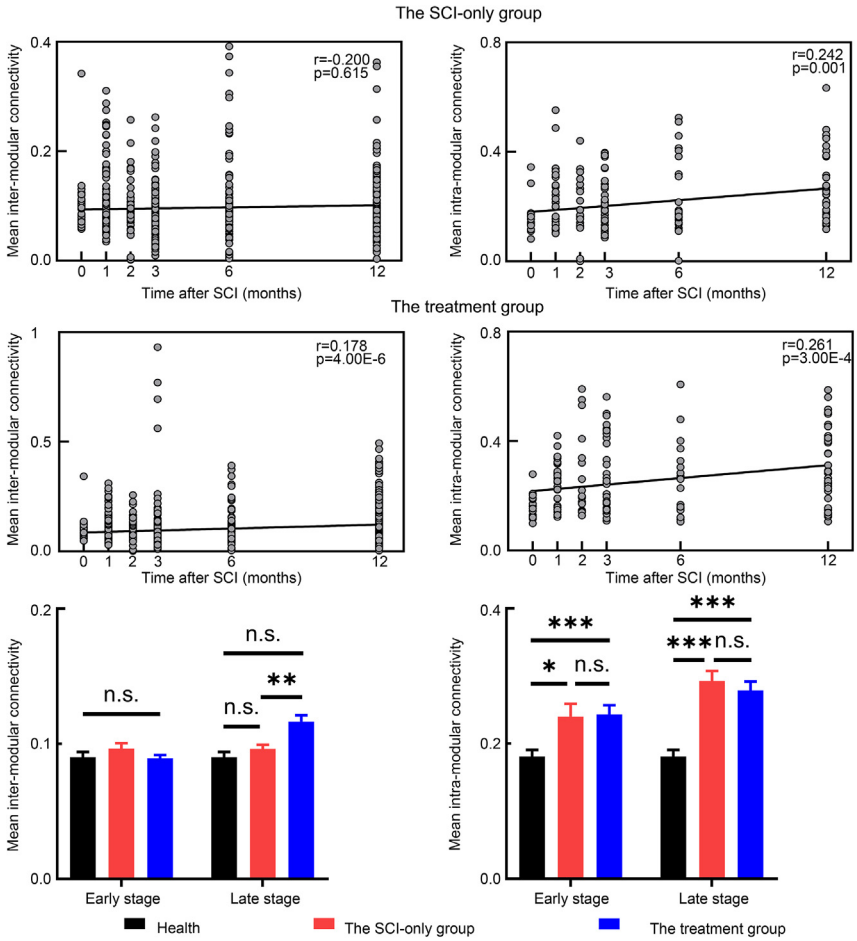

Figure 4. Post-SCI time-associated trajectories of mean intra- and inter-modular functional connectivity in the lesion-only and treatment groups

Significant between-group differences of mean intra- and inter-module functional connectivity strength in the early- and late-stages post-SCI are shown (all post-hocs: Games-Howell). *p < 0.05, **p < 0.01, ***p < 0.001. *n.s.*, none significance.

information was given in Table S1). By contrast, PC in the treatment group remained essentially normal, and only a significant decrease in PC was observed in the right insula in the early stage (p = 0.005; Figure 5).

Similarly, for FC in regions associated with the motor system, at the late stage, FC strengths between the left precentral gyrus and right postcentral gyrus, between the right precentral gyrus and right postcentral gyrus, and between the right precentral gyrus and right entorhinal area in the treatment group were higher than those in the SCI-only group (p = 0.013, p = 0.020, p = 0.040, respectively; Figure S2A). FC strength between the left precentral gyrus and right accessory basal nucleus of the amygdala in the SCI-only group was lower than that in the healthy period (p = 0.004; Figure S2A). In addition, at the late stage, FC in the treatment group between the right oral pontine reticular nucleus and right claustral amygdalar area, which functionally belongs to the cortical subplate nuclei was also clearly higher than that in the SCI-only group (p = 0.003; Figure S3).

For WM, the SCI-only group also displayed significant changes in the late stage (Figure 6; detailed data information was given in Table S2). Compared with the treatment group and the healthy period, the SCI-only group demonstrated significantly lower WM in the superior parietal lobule (p = 0.037) and left precuneus (p < 0.034); there was no difference among the three groups for WM in the right precuneus, whereas the SCI-only group showed significantly higher WM in the left ventral anterior nucleus of the thalamus (vs. healthy period: p = 0.112 × 10^{-3}, vs. treatment group: p = 0.047), left dentate nucleus (p = 0.045), and globose nucleus (p = 0.029) associated with sensory information integration.

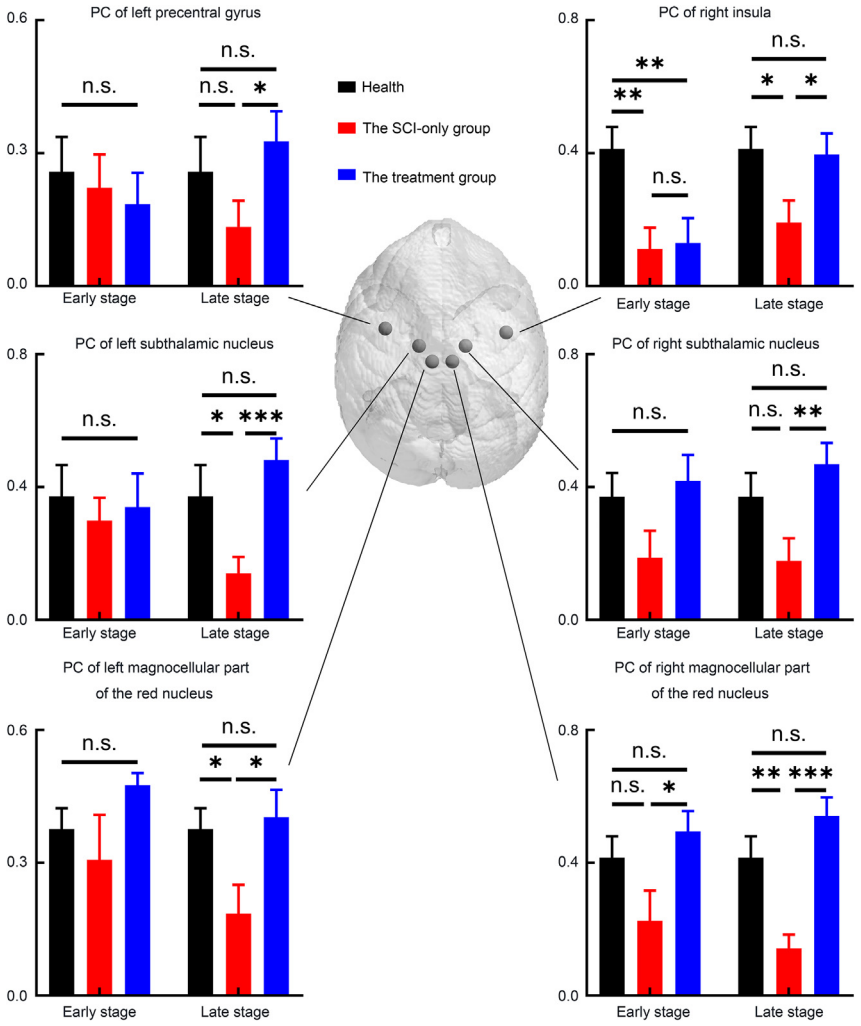

Figure 5. Significant differences in the participation coefficient among the SCI-only and treatment groups and health status

For multiple comparisons, LSD post-hoc was performed. *p < 0.05, **p < 0.01, ***p < 0.001. *n.s.*, none significance.

There were similar findings in FCs in regions associated with the sensory system; FC strengths between the right postcentral gyrus and left solitary nucleus, between the right postcentral gyrus and right solitary nucleus, and between the right postcentral gyrus and right superior parietal lobule in the SCI-only group were higher than those in the treatment group ($p = 0.029$, $p = 0.023$, $p = 0.011$, respectively; Figure S2B). Moreover, at the late stage, FC between the left postcentral gyrus and right nucleus of the diagonal band in the SCI-only group was lower than that in the treatment group ($p = 0.021$; Figure S2B). All FC data information and comparison results were shown in Table S3.

Receiver operating characteristics (ROC) analysis allows us to compare multiple acquisition strategies and multiple post-processing indices quantitatively and objectively.[33,34] ROC analysis for PC and WM of brain regions with statistically significant difference ($p < 0.001$) between the SCI-only group and treatment group was performed and results for the area under the ROC curve >0.7 were displayed. ROC analysis showed that the PC of the right magnocellular part of the red nucleus in the brain network could be the indicator that can best distinguish the SCI-only group and the treatment group. Thus, the magnocellular part of the red nucleus may reflect the best difference in brain remodeling induced by spontaneous compensation after SCI versus neural regeneration after NT3 treatment (Figure 7).

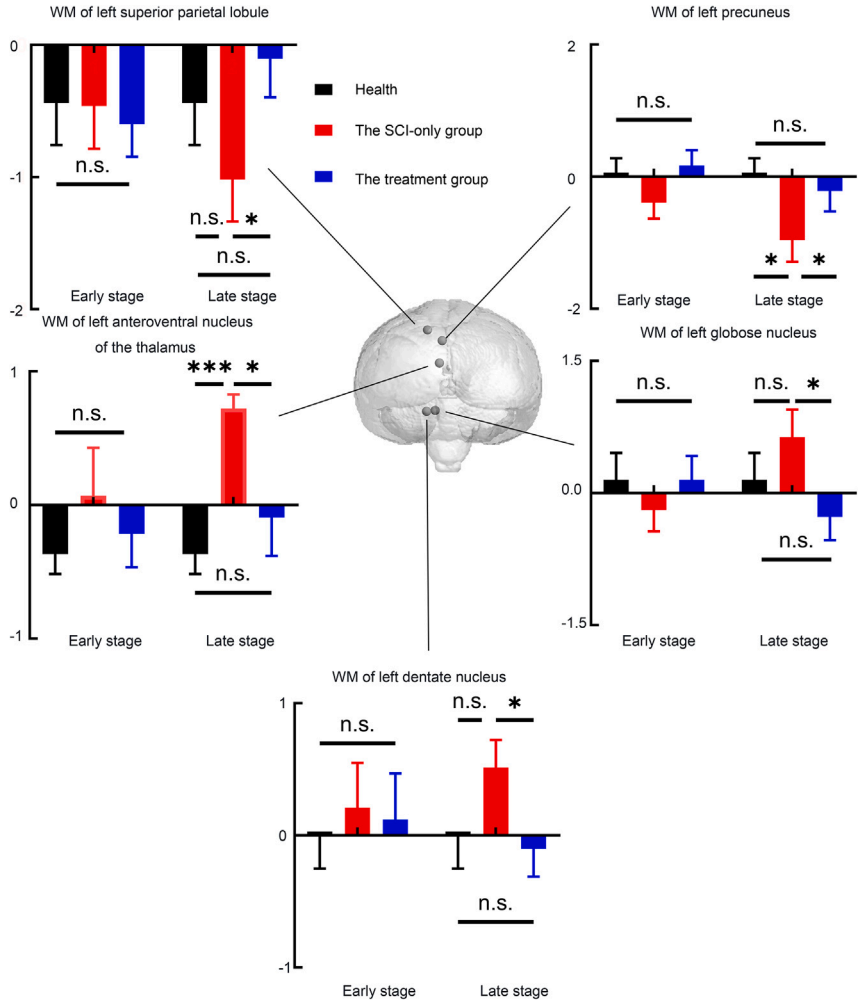

Figure 6. Significant differences in the within-module degree among the SCI-only and treatment groups and the health status

For left anteroventral nucleus of the thalamus, Games-Howell post-hoc multiple comparison was performed. For others, LSD post-hoc was performed. *p < 0.05, ***p < 0.001. *n.s.*, none significance.

The extent of spinal cord lesions and motor impairments

To assess the severity of injury, the ratio of the lesion area post-SCI to the spinal cord area in the healthy period was calculated for each animal. Results showed that there was no significant difference in the percentage of spinal damage area between the SCI-only and treatment groups at one month after operation, which proved the consistent degree of injury between the two groups. At 12 months post-SCI, however, a significant difference between the two groups was observed ($p = 0.003$; Figure S4A). The corresponding motor function of these animals was also analyzed. No difference of stride length was found at the healthy period and 2 months post-operation. But a significant recovery of stride length in the treated animals was observed at 12 months post-SCI compared to that in the SCI-only ones ($p = 0.013$; Figure S4B). The trajectories for time-dependent recovery from motor impairments on an individual basis were shown in Figure S4C.

DISCUSSION

The extent to which SCI can cause brain reorganization is unclear, and quantifying these reorganizations will help understand the cortical changes in the brain after SCI and NT3 treatment. Unlike previous beliefs that only a specific sensorimotor network is involved in SCI,[28,35] recent studies have found that SCI affects brain network regions or interconnected systems on a large scale.[21,32] Previous studies have used

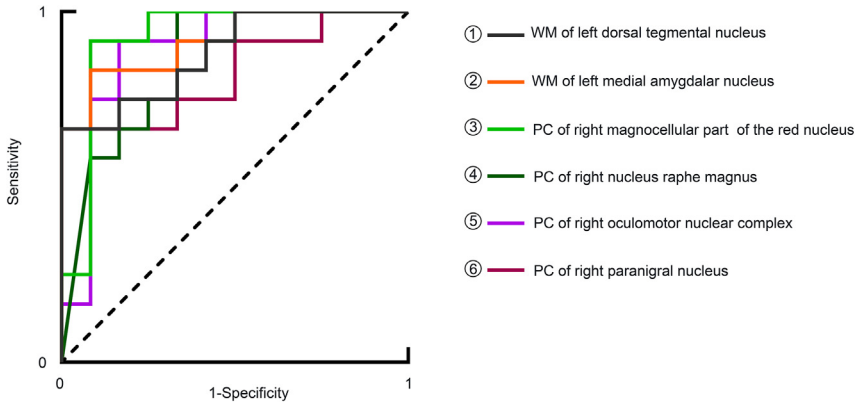

Figure 7. Receiver operation characteristic curves for discriminating functional changes of brain regions between the SCI-only and treatment groups

Areas under the lines represent the area under the curve (AUC), whereas black lines indicate random classification. The AUCs for the ROC of ①–⑥ are 0.882, 0.918, 0.924, 0.858, 0.889, and 0.785, respectively.

large-scale networks to analyze the modular organization of whole-brain resting-state FC networks in patients with complete SCI, demonstrating the potential application of the graph-theoretical method in assessing changes in brain network properties after SCI.

In this study, 470 ROIs were included to compare differences in large-scale network modules between animals in the SCI-only and treatment groups. By examining the modules and hubs of functional brain networks, we found the following findings: (1) Compared with the healthy period, the number of modules increased in the SCI-only and treatment groups at all postoperative time points. (2) The intra-modular FC strengths in the SCI-only and treatment groups at the early and late stages increased, and the mean intrahemispheric FC strength in the SCI-only group at the late stage increased. (3) The number of connector hubs in the SCI-only and treatment groups increased, whereas the number of provincial hubs decreased. (4) The affected brain regions of PC and WM after SCI and NT3 treatment were involved in areas related to sensorimotor control, cognition, and pain perception, such as insula, precentral gyrus, red nucleus, thalamus nucleus, and cerebellar nuclei. The magnocellular part of the red nucleus could distinguish the furthest distinct brain plasticity induced by spontaneous compensation after SCI and neural regeneration after NT3 treatment.

During the healthy period, the insula and primary somatosensory area were tightly functionally connected. Insula belonging to the salience network (SN) and the primary somatosensory area belonging to SMN belong to the same module. However, in the late stage after injury, the insula and primary somatosensory area were split into two modules, and the network separation of SN and SMN was found. A previous study about the network module after SCI demonstrated that the insula is in the same module as the precentral and postcentral gyrus in healthy controls, and the observations of our study were consistent with this finding.[32] The dissociation of these two networks in the late stage may reflect the loss of input from the extremities, leading to decreased spontaneous functional activity in primary sensorimotor cortical areas[36] and decreased demand for synchronized activation processing between brain regions. The insula, as a core node of the SN, is functionally and anatomically closely connected to the sensorimotor cortex[37,38] and is involved in information processing related to somatosensory and visual sensory stimulation. By contrast, in the late stage after SCI, a significant decrease in FC strength between the left insula and bilateral primary somatosensory areas occurred. This phenomenon indicated a loss of afferent information from the spinal cord to the primary somatosensory cortex, as well as reduced functional activity in the corresponding representative areas of the sensorimotor cortex. Moreover, synchronous activity was reduced between brain areas.[39,40]

In addition, low FC between the left insula and bilateral primary somatosensory areas in the SCI-only group was positively related to low NTPTs (increased pain signs), but restoring the FC after treatment can reduce pain signs, suggesting that NT3 treatment may relieve pain signs through reconnection of the insula. It was reported that the insula exerts a descending inhibitory effect on thermal nociception in the pain pathways of the

contralateral spinal dorsal horn.[41] The difference in the integrity of the descending pain regulation pathway may be one of the reasons for the distinct NTPTs between the SCI-only and treatment groups. As a node in the pain regulation neural circuits, the FC strength change of the insula may be a potential marker for pain signs.

Previous studies have demonstrated substantial spontaneous reorganization after SCI occurred in the subcortex, and new connections may compensate for damaged pathways connecting important motor areas.[42] One study found that the intrahemispheric FC strength of the primary sensorimotor cortex of patients with SCI increased, but interhemispheric FC strength did not increase,[39] which may be due to the limited ability of axonal long-distance spontaneous regeneration. In this study, consistent with previous results, we also observed that the mean intrahemispheric FC strength in the SCI-only group at the late stage was higher than that in the healthy period, but the mean interhemispheric FC strength was not significantly different. The increase in mean intrahemispheric FC may be associated with spontaneous plasticity after SCI, such as axonal sprouting to form new connections and projection patterns.[42] Although, in the late stage, there was no difference for mean left and right intrahemispheric FC strength post-SCI. There were significant differences among the three groups for WM in the left precuneus and mean FC strength between the left insula and bilateral somatosensory areas. Hemisection leads to lack of proprioception and fine tactile sensation information in the left hemisphere, which may disrupt the functional integration of DMN and reduce WM in the precuneus (a core node of DMN). Consistently, a significantly reduced regional homogeneity (ReHo) in the precuneus contralateral to injury has been reported.[43] The absence of nociception and temperature information in the right hemisphere had a minimal effect on these brain regions, suggesting that different kinds of sensory afferent loss lead to distinct brain network changes. To transfer information between different brain regions to perform various tasks, the integration and separation of networks is essential. FC strengths of whole-brain networks at the modular level in this study were analyzed to characterize the separation and integration of whole-brain networks. Compared with the healthy period, the mean intra-modular FC in both the early and late stages of the treatment group increased, suggesting that smaller cliques within brain network modules are more tightly connected after SCI to enhance the output of information and achieve the demands of sensory motor tasks.[28] In the late stage, the mean inter-modular FC strength in the treatment group was significantly higher than that in the SCI-only group, which could be partially attributed to NT3 treatment. Previous studies have shown that NT3 treatment can promote the recovery of sensorimotor information transmission.[14,44] Thus, the information flow between modules increased, and the functional integration of brain networks was enhanced after NT3 treatment. Furthermore, the mean intra-modular connectivity in the SCI-only group and the mean intra- and inter-modular connections in the treatment group increased with the injury time, suggesting that cortical function was affected continuously with the injury time.

Functional separation of brain networks can be thought to improve partly the ability of the brain to perform various tasks in parallel, and the separated modules contribute to the development of specific brain functions. In this study, WM and PC at the node level were calculated to describe the separation and specificity of functional modules. WM can be used to evaluate how well a node is connected to other nodes within the same module. In the late stage, the SCI-only group showed higher WM in the left ventral anterior nucleus of thalamic, dentate nucleus, globose nucleus, and superior parietal lobule than the treatment group. The high WM of these brain regions related to somatosensory reflected reduced input to the ipsilateral (right) primary somatosensory area after SCI; thus, the contralateral (left) somatosensory-related brain regions in the module played a major compensatory role. Given the imbalance of sensory input after SCI, the integrated reorganization of different thalamic subnuclei in the thalamocortical pathway and functional alterations in multiple sensory-related brain regions after SCI may provide a contribution and compensation for adaptive and non-adaptive cortical changes observed after SCI.[45] In this study, the SCI-only group showed significantly higher WM of the left ventral anterior nucleus of thalamic, dentate nucleus, and globose nucleus than the treatment group and the healthy period. This difference may be due to the lack of afferents from the lower motor center, which caused an imbalance of sensory inputs and a compensatory increase in WM. Brain regions associated with sensory integration likely spontaneously increase their regional and network functions to compensate for sensory dysfunction, and this compensatory effect is greater in the SCI-only group than in the treatment group. There were similar findings in FCs in regions associated with the sensory networks. Abnormal sensory responses were reported after SCI.[46] FC strength between the postcentral gyrus and nucleus of the diagonal band, which is specialized in the sensory processing of tactile stimuli, was significantly lower in the SCI-only group than that in the treatment group. This may reflect abnormal sensory responses to tactile stimuli post-SCI. In addition, extraspinal sensory pathways, such as a spinal cord bypassed vagal nerve pathway, may develop following injury.[47] In the SCI-only group, FC strength between the postcentral gyrus and solitary

nucleus, the main component of vagal nerves, was higher than other groups, which may reflect a developed spinal cord-bypass vagal nerve pathway to sustain sensory function. In addition, previous studies have shown an association between abnormal thalamic function and chronic pain.[48,49] Reorganization and integration of different thalamic subnuclei in the thalamocortical pathway after SCI may also be a factor for mood disorders and pain-processing deficits in patients with SCI.

Patients with SCI are 13 times more at risk for cognitive dysfunction than healthy people,[50] and up to 60% of patients with chronic SCI have deficits in attention, memory, and cognition.[51] The precuneus, as a core node of DMN, receives signals from the frontal, parietal, and temporal lobes. It is considered associated with a high level of cognitive function.[52,53] Our research showed that WM of the left precuneus in the SCI-only group was significantly lower than that in the treatment group and the healthy period, demonstrating that SCI can affect the DMN network and may contribute to cognitive decline after SCI.[43]

PC can be used to assess FC of nodes between modules. The treatment group showed greater PC in motor-related brain regions than the SCI-only group, such as bilateral globose nucleus, left precentral gyrus, right insula, and bilateral subthalamic nucleus, and it did not differ from the healthy period. This finding demonstrated that NT3 treatment could enhance information flows between brain regions and promote the integration of whole-brain motor functions to return to the healthy period. Sensorimotor activity has been shown to play a key role in functional recovery after partial SCI. In this study, FCs between the precentral gyrus and limbic system (entorhinal area and amygdala), between the precentral gyrus and postcentral gyrus, displayed stronger connections after treatment than SCI-only, suggesting treatment might restore the functional interaction of the motor network and promoting the improvement of motor function, such as stride length.

Notably, the present study found the magnocellular part of the red nucleus could distinguish the difference in brain network changes induced by spontaneous recovery after SCI and neuroregeneration after NT3 treatment. Following impairment of spinal axonal projections, retrograde axonal responses in the red nucleus may occur, typically involving chromatin dissolution and accumulation of neurofilaments, microtubules, and various membranous organelles[54] and related response of microglia to astrocytes.[55] Chromatinolysis, gliosis, and neuronal loss of the red nucleus occurred in brains of German shepherds with chronic degenerative myelopathy.[56] In this study, NT3 treatment inhibited inflammation, alleviated axonal degeneration, and promoted axonal regeneration. These markedly different pathological processes after SCI and NT3 treatment may explain why the magnocellular part of the red nucleus exhibited different PCs in the two groups of animals. The magnocellular part of the red nucleus preserved in the treatment group was involved more in the functional integration of brain networks, reflecting differences in brain network changes between the two groups of animals.

In conclusion, this study analyzed the changing processes of modularity in the functional brain network after SCI and NT3 treatment, revealed differences in brain modular connectivity after injury and treatment, and demonstrated the effect of NT3 treatment on improving SCI-induced dissociation in the brain network. These findings laid the foundation for further understanding the impact of SCI or neuroregeneration treatment on brain function and provide evidence for distinguishing between different subtypes of brain reorganization induced by spontaneous recovery and neuroregeneration. This work may help further guide the treatment of SCI.

Limitations of the study

This study had some limitations. First, the validity of the statistical analysis may be affected by the small number of animals. Second, further longitudinal changes with the injury time in topological properties (PC and WM) of nodes at the modular level were not analyzed. Subsequent research could expand the sample size and explore the changing processes of nodal topological properties in depth to reflect the plasticity of brain networks comprehensively. Third, performing MRI on animals usually requires anesthesia to obtain adequate immobilization.[57,58] The use of anesthetics may affect biochemical information, thereby masking or enlarging possible interactions between brain regions.[59] However, the reliability of test–retest results for longitudinal studies of fMRI activation and connectivity under anesthesia is reliable.[60] For this reason, the use of consistent anesthesia procedures and anesthetics in longitudinal studies allows data to be compared to show changes in brain network modules.

STAR★METHODS

Detailed methods are provided in the online version of this paper and include the following:

- KEY RESOURCES TABLE
- RESOURCE AVAILABILITY
  - Lead contact
  - Materials availability
  - Data and code availability
- EXPERIMENTAL MODEL AND SUBJECT DETAILS
  - Animals
  - Experimental model
- METHOD DETAILS
  - MRI scan
  - Data preprocessing
  - Functional network construction
  - Modularity
  - Hubs
  - Sensorimotor function evaluation
  - The extent of spinal cord lesions
- QUANTIFICATION AND STATISTICAL ANALYSIS

SUPPLEMENTAL INFORMATION

Supplemental information can be found online at https://doi.org/10.1016/j.isci.2023.106784.

ACKNOWLEDGMENTS

This work was supported by the National Natural Science Foundation of China [Grant nos. 31970970, 31900980, 82271403, 82272171, U21A20388, and 31730039], The Key Research and Development Program of Guangzhou [Grant no. 202206060003], Ministry of Science and Technology of China [Grant nos. 2019YFA0707103, 2020AAA0105601, and 2022ZD0211901], Chinese Academy of Sciences grant [Grant no. ZDBS-LY-SM028], Fundamental Research Funds for Central Public Welfare Research Institutes [Grant nos. 2021CZ-10, 2022CZ-12], and Fundamental Research Funds for the Central Universities [Grant no. YWF-22-L-811].

AUTHOR CONTRIBUTIONS

Conceptualization, J.S.R., C.Z., Z.X.L., Y.Z.Y., and X.G.L.; Methodology, T.F., C.Z., J.S.R., X.J.G., S.S.B., L.W.H., and Z.W.; Formal Analysis, T.F., C.Z., J.S.R., and S.S.B.; Writing – Original Draft, T.F., C.Z., and J.S.R.; Writing–Review & Editing, J.S.R., Z.X.L., Y.Z.Y., and X.G.L.; Funding Acquisition, J.S.R., C.Z., Z.X.L., Y.Z.Y., and X.G.L.; Resources, J.S.R., C.Z., Z.X.L., Y.Z.Y., and X.G.L.; Supervision, Z.X.L., Y.Z.Y., and X.G.L.

DECLARATION OF INTERESTS

The authors declare no competing interests.

Received: August 18, 2022
Revised: March 8, 2023
Accepted: April 26, 2023
Published: April 29, 2023

REFERENCES

1. Dietz, V., and Curt, A. (2006). Neurological aspects of spinal-cord repair: promises and challenges. Lancet Neurol. *5*, 688–694. https://doi.org/10.1016/s1474-4422(06)70522-1.

2. Mohammed, H., and Hollis, E.R., 2nd (2018). Cortical reorganization of sensorimotor systems and the role of intracortical circuits after spinal cord injury. Neurotherapeutics *15*, 588–603. https://doi.org/10.1007/s13311-018-0638-z.

3. Siddall, P.J., and Loeser, J.D. (2001). Pain following spinal cord injury. Spinal Cord *39*, 63–73. https://doi.org/10.1038/sj.sc.3101116.

4. Siddall, P.J., McClelland, J.M., Rutkowski, S.B., and Cousins, M.J. (2003). A longitudinal study of the prevalence and characteristics of pain in the first 5 years following spinal cord injury. Pain *103*, 249–257. https://doi.org/10.1016/s0304-3959(02)00452-9.

5. Dugan, E.A., Jergova, S., and Sagen, J. (2020). Mutually beneficial effects of intensive

exercise and GABAergic neural progenitor cell transplants in reducing neuropathic pain and spinal pathology in rats with spinal cord injury. Exp. Neurol. *327*, 113208. https://doi.org/10.1016/j.expneurol.2020.113208.

6. Zarei-Kheirabadi, M., Sadrosadat, H., Mohammadshirazi, A., Jaberi, R., Sorouri, F., Khayyatan, F., and Kiani, S. (2020). Human embryonic stem cell-derived neural stem cells encapsulated in hyaluronic acid promotes regeneration in a contusion spinal cord injured rat. Int. J. Biol. Macromol. *148*, 1118–1129. https://doi.org/10.1016/j.ijbiomac.2020.01.219.

7. Zhong, D., Cao, Y., Li, C.J., Li, M., Rong, Z.J., Jiang, L., Guo, Z., Lu, H.B., and Hu, J.Z. (2020). Neural stem cell-derived exosomes facilitate spinal cord functional recovery after injury by promoting angiogenesis. Exp. Biol. Med. *245*, 54–65. https://doi.org/10.1177/1535370219895491.

8. Kim, D.H., and Jahng, T.A. (2004). Continuous brain-derived neurotrophic factor (BDNF) infusion after methylprednisolone treatment in severe spinal cord injury. J. Kor. Med. Sci. *19*, 113–122. https://doi.org/10.3346/jkms.2004.19.1.113.

9. Shroff, G., Dhanda Titus, J., and Shroff, R. (2017). A review of the emerging potential therapy for neurological disorders: human embryonic stem cell therapy. Am. J. Stem Cells *6*, 1–12.

10. Wang, G., Wang, X., and Huang, L. (2017). Feasibility of chitosan-alginate (Chi-Alg) hydrogel used as scaffold for neural tissue engineering: a pilot study in vitro. Biotechnol. Biotechnol. Equip. *31*, 1–8. https://doi.org/10.1080/13102818.2017.1332493.

11. Hu, Y., Zhang, F., Zhong, W., Liu, Y., He, Q., Yang, M., Chen, H., Xu, X., Bian, K., Xu, J., et al. (2019). Transplantation of neural scaffolds consisting of dermal fibroblast-reprogrammed neurons and 3D silk fibrous materials promotes the repair of spinal cord injury. J. Mater. Chem. B *7*, 7525–7539. https://doi.org/10.1039/c9tb01929d.

12. Koffler, J., Zhu, W., Qu, X., Platoshyn, O., Dulin, J.N., Brock, J., Graham, L., Lu, P., Sakamoto, J., Marsala, M., et al. (2019). Biomimetic 3D-printed scaffolds for spinal cord injury repair. Nat. Med. *25*, 263–269. https://doi.org/10.1038/s41591-018-0296-z.

13. Liu, D., Li, X., Xiao, Z., Yin, W., Zhao, Y., Tan, J., Chen, B., Jiang, X., and Dai, J. (2019). Different functional bio-scaffolds share similar neurological mechanism to promote locomotor recovery of canines with complete spinal cord injury. Biomaterials *214*, 119230. https://doi.org/10.1016/j.biomaterials.2019.119230.

14. Rao, J.S., Zhao, C., Zhang, A., Duan, H., Hao, P., Wei, R.H., Shang, J., Zhao, W., Liu, Z., Yu, J., et al. (2018). NT3-chitosan enables de novo regeneration and functional recovery in monkeys after spinal cord injury. Proc. Natl. Acad. Sci. USA *115*, E5595–E5604. https://doi.org/10.1073/pnas.1804735115.

15. Cramer, S.C., Lastra, L., Lacourse, M.G., and Cohen, M.J. (2005). Brain motor system function after chronic, complete spinal cord injury. Brain *128*, 2941–2950. https://doi.org/10.1093/brain/awh648.

16. Curt, A., Alkadhi, H., Crelier, G.R., Boendermaker, S.H., Hepp-Reymond, M.C., and Kollias, S.S. (2002). Changes of non-affected upper limb cortical representation in paraplegic patients as assessed by fMRI. Brain *125*, 2567–2578. https://doi.org/10.1093/brain/awf250.

17. Endo, T., Spenger, C., Tominaga, T., Brené, S., and Olson, L. (2007). Cortical sensory map rearrangement after spinal cord injury: fMRI responses linked to Nogo signalling. Brain *130*, 2951–2961. https://doi.org/10.1093/brain/awm237.

18. Freund, P., Weiskopf, N., Ward, N.S., Hutton, C., Gall, A., Ciccarelli, O., Craggs, M., Friston, K., and Thompson, A.J. (2011). Disability, atrophy and cortical reorganization following spinal cord injury. Brain *134*, 1610–1622. https://doi.org/10.1093/brain/awr093.

19. Karunakaran, K.D., Yuan, R., He, J., Zhao, J., Cui, J.L., Zang, Y.F., Zhang, Z., Alvarez, T.L., and Biswal, B.B. (2020). Resting-state functional connectivity of the thalamus in complete spinal cord injury. Neurorehabilitation Neural Repair *34*, 122–133. https://doi.org/10.1177/1545968319893299.

20. Zheng, W., Wang, L., Chen, Q., Li, X., Chen, X., Qin, W., Li, K., Lu, J., and Chen, N. (2021). Functional reorganizations outside the sensorimotor regions following complete thoracolumbar spinal cord injury. J. Magn. Reson. Imag. *54*, 1551–1559. https://doi.org/10.1002/jmri.27764.

21. Min, Y.S., Chang, Y., Park, J.W., Lee, J.M., Cha, J., Yang, J.J., Kim, C.H., Hwang, J.M., Yoo, J.N., and Jung, T.D. (2015). Change of brain functional connectivity in patients with spinal cord injury: graph theory based approach. Ann. Rehabil. Med. *39*, 374–383. https://doi.org/10.5535/arm.2015.39.3.374.

22. Rao, J.S., Liu, Z., Zhao, C., Wei, R.H., Zhao, W., Yang, Z.Y., and Li, X.G. (2016). Longitudinal evaluation of functional connectivity variation in the monkey sensorimotor network induced by spinal cord injury. Acta Physiol. *217*, 164–173. https://doi.org/10.1111/apha.12645.

23. Bullmore, E., and Sporns, O. (2009). Complex brain networks: graph theoretical analysis of structural and functional systems. Nat. Rev. Neurosci. *10*, 186–198. https://doi.org/10.1038/nrn2575.

24. Rubinov, M., and Sporns, O. (2010). Complex network measures of brain connectivity: uses and interpretations. Neuroimage *52*, 1059–1069. https://doi.org/10.1016/j.neuroimage.2009.10.003.

25. Khatri, U., and Kwon, G.R. (2022). Alzheimer's disease diagnosis and biomarker analysis using resting-state functional MRI functional brain network with multi-measures features and hippocampal subfield and amygdala volume of structural MRI. Front. Aging Neurosci. *14*, 818871. https://doi.org/10.3389/fnagi.2022.818871.

26. Oishi, K., Mielke, M.M., Albert, M., Lyketsos, C.G., and Mori, S. (2011). DTI analyses and clinical applications in Alzheimer's disease. J. Alzheimers Dis. *26*, 287–296. https://doi.org/10.3233/JAD-2011-0007.

27. Drenthen, G.S., Fasen, F., Fonseca Wald, E.L.A., Backes, W.H., Aldenkamp, A.P., Vermeulen, R.J., Debeij-van Hall, M., Hendriksen, J., Klinkenberg, S., and Jansen, J.F.A. (2020). Functional brain network characteristics are associated with epilepsy severity in childhood absence epilepsy. Neuroimage. Clin. *27*, 102264. https://doi.org/10.1016/j.nicl.2020.102264.

28. Hawasli, A.H., Rutlin, J., Roland, J.L., Murphy, R.K.J., Song, S.K., Leuthardt, E.C., Shimony, J.S., and Ray, W.Z. (2018). Spinal cord injury disrupts resting-state networks in the human brain. J. Neurotrauma *35*, 864–873. https://doi.org/10.1089/neu.2017.5212.

29. Kaushal, M., Oni-Orisan, A., Chen, G., Li, W., Leschke, J., Ward, B.D., Kalinosky, B., Budde, M.D., Schmit, B.D., Li, S.J., et al. (2017). Evaluation of whole-brain resting-state functional connectivity in spinal cord injury: a large-scale network analysis using network-based statistic. J. Neurotrauma *34*, 1278–1282. https://doi.org/10.1089/neu.2016.4649.

30. He, Y., Wang, J., Wang, L., Chen, Z.J., Yan, C., Yang, H., Tang, H., Zhu, C., Gong, Q., Zang, Y., and Evans, A.C. (2009). Uncovering intrinsic modular organization of spontaneous brain activity in humans. PLoS One *4*, e5226. https://doi.org/10.1371/journal.pone.0005226.

31. Power, J.D., Schlaggar, B.L., Lessov-Schlaggar, C.N., and Petersen, S.E. (2013). Evidence for hubs in human functional brain networks. Neuron *79*, 798–813. https://doi.org/10.1016/j.neuron.2013.07.035.

32. Kaushal, M., Oni-Orisan, A., Chen, G., Li, W., Leschke, J., Ward, D., Kalinosky, B., Budde, M., Schmit, B., Li, S.J., et al. (2017). Large-scale network analysis of whole-brain resting-state functional connectivity in spinal cord injury: a comparative study. Brain Connect. *7*, 413–423. https://doi.org/10.1089/brain.2016.0468.

33. Constable, R.T., Skudlarski, P., and Gore, J.C. (1995). An ROC approach for evaluating functional brain MR imaging and postprocessing protocols. Magn. Reson. Med. *34*, 57–64. https://doi.org/10.1002/mrm.1910340110.

34. Fawcett, T. (2006). An introduction to ROC analysis. Pattern Recogn. Lett. *27*, 861–874. https://doi.org/10.1016/j.patrec.2005.10.010.

35. Athanasiou, A., Klados, M.A., Pandria, N., Foroglou, N., Kavazidi, K.R., Polyzoidis, K., and Bamidis, P.D. (2017). A systematic review of investigations into functional brain connectivity following spinal cord injury. Front. Hum. Neurosci. *11*, 517. https://doi.org/10.3389/fnhum.2017.00517.

36. Yagüe, J.G., Humanes-Valera, D., Aguilar, J., and Foffani, G. (2014). Functional reorganization of the forepaw cortical representation immediately after thoracic spinal cord hemisection in rats. Exp. Neurol.

257, 19–24. https://doi.org/10.1016/j.expneurol.2014.03.015.

37. Addicott, M.A., Sweitzer, M.M., Froeliger, B., Rose, J.E., and McClernon, F.J. (2015). Increased functional connectivity in an insula-based network is associated with improved smoking cessation outcomes. Neuropsychopharmacology *40*, 2648–2656. https://doi.org/10.1038/npp.2015.114.

38. Jakab, A., Molnár, P.P., Bogner, P., Béres, M., and Berényi, E.L. (2012). Connectivity-based parcellation reveals interhemispheric differences in the insula. Brain Topogr. *25*, 264–271. https://doi.org/10.1007/s10548-011-0205-y.

39. Hou, J.M., Sun, T.S., Xiang, Z.M., Zhang, J.Z., Zhang, Z.C., Zhao, M., Zhong, J.F., Liu, J., Zhang, H., Liu, H.L., et al. (2014). Alterations of resting-state regional and network-level neural function after acute spinal cord injury. Neuroscience *277*, 446–454. https://doi.org/10.1016/j.neuroscience.2014.07.045.

40. Jurkiewicz, M.T., Mikulis, D.J., McIlroy, W.E., Fehlings, M.G., and Verrier, M.C. (2007). Sensorimotor cortical plasticity during recovery following spinal cord injury: a longitudinal fMRI study. Neurorehabilitation Neural Repair *21*, 527–538. https://doi.org/10.1177/1545968307301872.

41. You, H.J., Lei, J., and Pertovaara, A. (2022). Thalamus: the 'promoter' of endogenous modulation of pain and potential therapeutic target in pathological pain. Neurosci. Biobehav. Rev. *139*, 104745. https://doi.org/10.1016/j.neubiorev.2022.104745.

42. Ramu, J., Herrera, J., Grill, R., Bockhorst, T., and Narayana, P. (2008). Brain fiber tract plasticity in experimental spinal cord injury: diffusion tensor imaging. Exp. Neurol. *212*, 100–107. https://doi.org/10.1016/j.expneurol.2008.03.018.

43. Rao, J.S., Ma, M., Zhao, C., Liu, Z., Yang, Z.Y., and Li, X.G. (2015). Alteration of brain regional homogeneity of monkeys with spinal cord injury: a longitudinal resting-state functional magnetic resonance imaging study. Magn. Reson. Imaging *33*, 1156–1162. https://doi.org/10.1016/j.mri.2015.06.011.

44. Rao, J.S., Zhao, C., Wei, R.H., Feng, T., Bao, S.S., Zhao, W., Tian, Z., Liu, Z., Yang, Z.Y., and Li, X.G. (2022). Neural regeneration therapy after spinal cord injury induces unique brain functional reorganizations in rhesus monkeys. Ann. Med. *54*, 1867–1883. https://doi.org/10.1080/07853890.2022.2089728.

45. Shipp, S. (2003). The functional logic of cortico-pulvinar connections. Philos. Trans. R. Soc. Lond. B Biol. Sci. *358*, 1605–1624. https://doi.org/10.1098/rstb.2002.1213.

46. Bian, D., Ossipov, M.H., Zhong, C., Malan, T.P., Jr., and Porreca, F. (1998). Tactile allodynia, but not thermal hyperalgesia, of the hindlimbs is blocked by spinal transection in rats with nerve injury. Neurosci. Lett. *241*, 79–82. https://doi.org/10.1016/s0304-3940(98)00051-2.

47. Krhut, J., Tintera, J., Bilkova, K., Holy, P., Zachoval, R., Zvara, P., and Blok, B. (2017). Brain activity on fMRI associated with urinary bladder filling in patients with a complete spinal cord injury. Neurourol. Urodyn. *36*, 155–159. https://doi.org/10.1002/nau.22901.

48. Gustin, S.M., Wrigley, P.J., Youssef, A.M., McIndoe, L., Wilcox, S.L., Rae, C.D., Edden, R.A.E., Siddall, P.J., and Henderson, L.A. (2014). Thalamic activity and biochemical changes in individuals with neuropathic pain after spinal cord injury. Pain *155*, 1027–1036. https://doi.org/10.1016/j.pain.2014.02.008.

49. Whitt, J.L., Masri, R., Pulimood, N.S., and Keller, A. (2013). Pathological activity in mediodorsal thalamus of rats with spinal cord injury pain. J. Neurosci. *33*, 3915–3926. https://doi.org/10.1523/jneurosci.2639-12.2013.

50. Craig, A., Guest, R., Tran, Y., and Middleton, J. (2017). Cognitive impairment and mood states after spinal cord injury. J. Neurotrauma *34*, 1156–1163. https://doi.org/10.1089/neu.2016.4632.

51. Chiaravalloti, N.D., Weber, E., Wylie, G., Dyson-Hudson, T., and Wecht, J.M. (2020). Patterns of cognitive deficits in persons with spinal cord injury as compared with both age-matched and older individuals without spinal cord injury. J. Spinal Cord Med. *43*, 88–97. https://doi.org/10.1080/10790268.2018.1543103.

52. Bakola, S., Gamberini, M., Passarelli, L., Fattori, P., and Galletti, C. (2010). Cortical connections of parietal field PEc in the macaque: linking vision and somatic sensation for the control of limb action. Cerebr. Cortex *20*, 2592–2604. https://doi.org/10.1093/cercor/bhq007.

53. Mantini, D., Gerits, A., Nelissen, K., Durand, J.B., Joly, O., Simone, L., Sawamura, H., Wardak, C., Orban, G.A., Buckner, R.L., and Vanduffel, W. (2011). Default mode of brain function in monkeys. J. Neurosci. *31*, 12954–12962. https://doi.org/10.1523/JNEUROSCI.2318-11.2011.

54. Aldskogius, H., and Arvidsson, J. (1978). Nerve cell degeneration and death in the trigeminal ganglion of the adult rat following peripheral nerve transection. J. Neurocytol. *7*, 229–250. https://doi.org/10.1007/bf01217921.

55. Tseng, G.F., Wang, Y.J., and Lai, Q.C. (1996). Rubral astrocytic reactions to proximal and distal axotomy of rubrospinal neurons in the rat. Brain Res. *742*, 115–128. https://doi.org/10.1016/s0006-8993(96)00972-9.

56. Johnston, P.E., Barrie, J.A., McCulloch, M.C., Anderson, T.J., and Griffiths, I.R. (2000). Central nervous system pathology in 25 dogs with chronic degenerative radiculomyelopathy. Vet. Rec. *146*, 629–633. https://doi.org/10.1136/vr.146.22.629.

57. Paasonen, J., Salo, R.A., Shatillo, A., Forsberg, M.M., Närväinen, J., Huttunen, J.K., and Gröhn, O. (2016). Comparison of seven different anesthesia protocols for nicotine pharmacologic magnetic resonance imaging in rat. Eur. Neuropsychopharmacol *26*, 518–531. https://doi.org/10.1016/j.euroneuro.2015.12.034.

58. Ailiani, A.C., Neuberger, T., Brasseur, J.G., Banco, G., Wang, Y., Smith, N.B., and Webb, A.G. (2014). Quantifying the effects of inactin vs Isoflurane anesthesia on gastrointestinal motility in rats using dynamic magnetic resonance imaging and spatio-temporal maps. Neuro Gastroenterol. Motil. *26*, 1477–1486. https://doi.org/10.1111/nmo.12410.

59. Bonhomme, V., Staquet, C., Montupil, J., Defresne, A., Kirsch, M., Martial, C., Vanhaudenhuyse, A., Chatelle, C., Larroque, S.K., Raimondo, F., et al. (2019). General anesthesia: a probe to explore consciousness. Front. Syst. Neurosci. *13*, 36. https://doi.org/10.3389/fnsys.2019.00036.

60. Vedaei, F., Alizadeh, M., Romo, V., Mohamed, F.B., and Wu, C. (2022). The effect of general anesthesia on the test-retest reliability of resting-state fMRI metrics and optimization of scan length. Front. Neurosci. *16*, 937172. https://doi.org/10.3389/fnins.2022.937172.

61. Rohlfing, T., Kroenke, C.D., Sullivan, E.V., Dubach, M.F., Bowden, D.M., Grant, K.A., and Pfefferbaum, A. (2012). The INIA19 template and NeuroMaps atlas for primate brain image parcellation and spatial normalization. Front. Neuroinf. *6*, 27. https://doi.org/10.3389/fninf.2012.00027.

62. Chai, X.J., Castañón, A.N., Ongür, D., and Whitfield-Gabrieli, S. (2012). Anticorrelations in resting state networks without global signal regression. Neuroimage *59*, 1420–1428. https://doi.org/10.1016/j.neuroimage.2011.08.048.

63. Murphy, K., Birn, R.M., Handwerker, D.A., Jones, T.B., and Bandettini, P.A. (2009). The impact of global signal regression on resting state correlations: are anti-correlated networks introduced? Neuroimage *44*, 893–905. https://doi.org/10.1016/j.neuroimage.2008.09.036.

64. Murphy, K., and Fox, M.D. (2017). Towards a consensus regarding global signal regression for resting state functional connectivity MRI. Neuroimage *154*, 169–173. https://doi.org/10.1016/j.neuroimage.2016.11.052.

65. Wen, X., Zhang, H., Li, G., Liu, M., Yin, W., Lin, W., Zhang, J., and Shen, D. (2019). First-year development of modules and hubs in infant brain functional networks. Neuroimage *185*, 222–235. https://doi.org/10.1016/j.neuroimage.2018.10.019.

66. Cohen, J.R., and D'Esposito, M. (2016). The segregation and integration of distinct brain networks and their relationship to cognition. J. Neurosci. *36*, 12083–12094. https://doi.org/10.1523/JNEUROSCI.2965-15.2016.

67. Sporns, O., and Betzel, R.F. (2016). Modular brain networks. Annu. Rev. Psychol. *67*, 613–640. https://doi.org/10.1146/annurev-psych-122414-033634.

68. Clauset, A., Newman, M.E.J., and Moore, C. (2004). Finding community structure in very large networks. Phys. Rev. E - Stat. Nonlinear Soft Matter Phys. *70*, 066111. https://doi.org/10.1103/PhysRevE.70.066111.

69. Najafi, M., McMenamin, B.W., Simon, J.Z., and Pessoa, L. (2016). Overlapping communities reveal rich structure in large-scale brain networks during rest and task conditions. Neuroimage *135*, 92–106. https://doi.org/10.1016/j.neuroimage.2016.04.054.

70. Yeo, B.T.T., Krienen, F.M., Chee, M.W.L., and Buckner, R.L. (2014). Estimates of segregation and overlap of functional connectivity networks in the human cerebral cortex. Neuroimage *88*, 212–227. https://doi.org/10.1016/j.neuroimage.2013.10.046.

71. Tang, W., Jbabdi, S., Zhu, Z., Cottaar, M., Grisot, G., Lehman, J.F., Yendiki, A., and Haber, S.N. (2019). A connectional hub in the rostral anterior cingulate cortex links areas of emotion and cognitive control. Elife *8*, e43761. https://doi.org/10.7554/eLife.43761.

72. Bullmore, E., and Sporns, O. (2012). The economy of brain network organization. Nat. Rev. Neurosci. *13*, 336–349. https://doi.org/10.1038/nrn3214.

73. Guimerà, R., Mossa, S., Turtschi, A., and Amaral, L.A.N. (2005). The worldwide air transportation network: anomalous centrality, community structure, and cities' global roles. Proc. Natl. Acad. Sci. USA *102*, 7794–7799. https://doi.org/10.1073/pnas.0407994102.

74. Bertolero, M.A., Yeo, B.T.T., and D'Esposito, M. (2015). The modular and integrative functional architecture of the human brain. Proc. Natl. Acad. Sci. USA *112*, E6798–E6807. https://doi.org/10.1073/pnas.1510619112.

75. Chong, J.S.X., Ng, K.K., Tandi, J., Wang, C., Poh, J.H., Lo, J.C., Chee, M.W.L., and Zhou, J.H. (2019). Longitudinal changes in the cerebral cortex functional organization of healthy elderly. J. Neurosci. *39*, 5534–5550. https://doi.org/10.1523/JNEUROSCI.1451-18.2019.

76. Cole, M.W., Reynolds, J.R., Power, J.D., Repovs, G., Anticevic, A., and Braver, T.S. (2013). Multi-task connectivity reveals flexible hubs for adaptive task control. Nat. Neurosci. *16*, 1348–1355. https://doi.org/10.1038/nn.3470.

77. Guimerà, R., Sales-Pardo, M., and Amaral, L.A.N. (2007). Classes of complex networks defined by role-to-role connectivity profiles. Nat. Phys. *3*, 63–69. https://doi.org/10.1038/nphys489.

STAR★METHODS

KEY RESOURCES TABLE

REAGENT or RESOURCE	SOURCE	IDENTIFIER
Chemicals, peptides, and recombinant proteins		
Ketamine	Provet	Keti1
Xylazine	GlpBio	GC17296
Sodium pentobarbital	New Asia Pharmaceutical	H31021724
Penicillin	Heowns	P-0278447
Pentazocine	CR Double-Crane	H10983218
Atropine	Jinyao Pharmaceutical	H12020382
Propofol	Libang Pharmaceutical	1203091
Experimental models: Organisms/strains		
Rhesus macaques	Laboratory Animal Resource Research Center, CAMS & PUMC	XC21001
Software and algorithms		
Prism	Graphpad	8.3
SPSS	Microsoft	20.0
Matlab	MathWorks, Natick, MA, USA	R2017a
Brain Connectivity Toolbox	http://www.brain-connectivity-toolbox.net	RRID: SCR_004841
SPM 12	The Wellcome Center for Human Neuroimaging	http://www.fil.ion.ucl.ac.uk/spm/software/spm12/
DPARSF	http://restfmri.net/forum/DPARSF	RRID: SCR_002372
Other		
3T Siemens MR system	Siemens, Erlangen, Germany	N/A
The Vicon system	Oxford Metrics Limited Company, Dayton, UK	N/A
The laser stimulator	BWT Beijing Ltd, Beijing, CN	N/A

RESOURCE AVAILABILITY

Lead contact

Further information and requests for resources and reagents should be directed to and will be fulfilled by the lead contact, Jia-Sheng Rao (raojschina@126.com).

Materials availability

This study did not generate unique reagents.

Data and code availability

All data reported in this paper will be shared by the lead contact upon request.

This paper does not report original code.

Any additional information required to reanalyse the data reported in this paper is available from the lead contact upon request.

EXPERIMENTAL MODEL AND SUBJECT DETAILS

Animals

Eight adult female rhesus monkeys (mean weight: 5 ± 1 kg, mean age: 5–6 years old) with good coordination and low aggression were chosen in this study. The animals were randomly divided into two groups: the

SCI-only group and the treatment group. The experimental procedure was approved by the Biological and Medical Ethics Committee of Beihang University (BM20180046). All animal experiments were performed in accordance with the ARRIVE guidelines.

Experimental model

All monkeys were kept alone in a room with controlled temperature and humidity. Food and water were freely available, and fresh fruit was provided daily. Anesthesia was administered by intramuscular injection of ketamine hydrochloride solution (10 mg/kg) before surgery and then maintained by intramuscular injection of xylazine hydrochloride (5 mg/kg). And then maintained with sodium pentobarbital (20 mg/kg) by an intravenous drip. The right spinal cord hemi-transection model was performed using laminectomy at the T7–T9 thoracic vertebrae. Under a surgical microscope, the tissue (10 mm long and 2–3 mm wide) was removed at 0.5 mm right of the posterior central vein of the spinal cord for all animals. After topical hemostasis, the repair materials with corresponding size were implanted into the SCI area of the animals in the treatment group. All animals were given daily antibiotics (penicillin 240 mg per day) and painkillers (pentazocine 2 mg/kg) for 5 days postoperatively.

METHOD DETAILS

MRI scan

All data were acquired via a custom-made four-channel primate head transmitter receiver coil on a 3T Siemens MR system (Magnetom Skyra, Siemens, Erlangen, Germany). Scanning was executed at healthy period (baseline) and 1, 2, 3, 6, and 12 months post-SCI.

Anesthesia was induced by intramuscular injection of ketamine hydrochloride solution (10 mg/kg) before scanning, and atropine sulfate was injected intramuscularly (0.05 mg/kg) to reduce salivary secretion. Anesthesia was maintained by intravenous puncture with a mixed saline solution of propofol (0.25 mg/kg/min) and ketamine (0.03 mg/kg/min). All animals were placed in the prone position.

Functional data were obtained using the gradient echo-echo planar imaging sequence (GRE-EPI) with the following imaging parameters: repetition time (TR)/echo time (TE) = 2000 ms/30 ms; field of view = 128 × 128 mm; matrix = 64 × 64; slice thickness = 2 mm; and flip angle = 90°. A total of 25 consecutive slices of axial images covering the whole brain were collected. Scanning lasted for 4 min to obtain 120 volumes of data.

Structural data were obtained via the 3D magnetization-prepared rapid acquisition gradient echo sequence with the following imaging parameters: TR/TE = 1520 ms/4.42 ms; flip angle = 15°; inversion time (TI) = 520 ms; and 240 consecutive slices to cover the whole brain with an isotropic voxel size of 0.5 mm^3.

Spinal cord structural images were acquired by proton-density weighted sequence with the following parameters: TR = 3050 ms; TE = 11 ms; flip angle = 15°; matrix = 320 × 320; field of view = 196 × 196 mm, and resolution = 0.6 × 0.6 × 2.0 mm^3. Scanning center was located at the surgical position of the spinal cord, and 27 consecutive slices of axial images covering the SCI region were collected.

Data preprocessing

The non-task state fMRI data under anesthesia were preprocessed with Data Processing Assistant for Resting-State fMRI (http://restfmri.net/forum/DPARSF), which is based on Statistical Parametric Mapping (SPM12) (http://www.fil.ion.ucl.ac.uk/spm/software/spm12/). First, the first 10 volumes of each functional time series were removed due to signal equilibrium. Second, we conducted slice timing correction on the remaining 110 vol Head motion between volumes was evaluated and corrected using rigid body registration, and we excluded datasets with maximum translation exceeding 2 mm, with the maximum rotation exceeding 2°. On the basis of the standard stereotaxic coordinate system, we spatially normalized the corrected fMRI images to the space of the INIA19 primate brain atlas by using T1 images unified segmentation. Each voxel was resampled to isotropic 0.5 × 0.5 × 0.5 mm^3. The images were then smoothed with a Gaussian kernel with a 6-mm full-width half-maximum Gaussian kernel. To remove the possible variances from the time course of each voxel (including global signals and signals from white matter and

cerebrospinal fluid), we regressed the nuisance covariates. Finally, a bandpass filter (0.01–0.1 Hz) was applied to reduce the low-frequency drifts and high-frequency noise.

Functional network construction

We first parcellated the whole brain into 470 cortical and subcortical regions according to the INIA19 primate brain atlas[61] except for white matter regions. The time series in each region of interest (ROI) was obtained by averaging the time series of all voxels within the ROI. Edges of the correlation matrix were measured by computing Pearson's correlation coefficients between the preprocessed time series of every pair of ROIs. Given the obscure explanation of negative correlations,[62–64] the modularity analysis was only performed on positive correlations.[65]

For statistical purposes, Pearson's correlation coefficients between each pair of nodes were transformed into Fisher's z scores. Accordingly, for each animal, we obtained a 470 × 470 symmetric positive FC matrix. All matrices obtained for animals in each group at each time point were averaged to generate the group-level FC matrix. To compare the SCI-only group and the treatment group under the condition of the same cost, a range of cost thresholds from 0.10 to 0.50 with 0.01 as an increment was applied to the matrix, with the cost defined as the ratio of the number of edges to the total number of possible edges. In addition, ROI-based FC analyses were performed by defining the left and right precentral gyrus, postcentral gyrus as ROIs and calculating FC between the ROI and other brain regions within the whole brain to investigate the functional integration patterns in region association with the sensorimotor system. FC in the oral pontine reticular nucleus was calculated and analyzed to observe cortico-reticular connectivity.

Modularity

Modularity is an important feature for complex brain networks, and modules refer to clusters of nodes with high within-module connectivity and low between-module connectivity.[23] Module is defined as a community, the inside of which has denser connections than the rest of the network. Several algorithms have been developed to detect those modules. The basic approach is to measure the maximum modularity value Q. High Q scores mean highly modular networks, which contain segregated modules and few inter-modular connections.[66,67]

To investigate modular-level topological disruptions, the greedy algorithm[68] was used to measure the maximum modularity value, Q, which is defined as follows:

$$Q = \frac{1}{2m}\sum_{i,j}\left[A_{ij} - \frac{k_i k_j}{2m}\right]\delta\left(c_i, c_j\right)$$

where A_{ij} is the FC strength connecting the nodes i and j, and $m = \frac{1}{2}\sum_{ij}A_{ij}$. k_i represents the sum of FC strength connecting node i, c_j is the module that node j belongs to, and δ (u, v) is equal to 1 if u = v and 0 otherwise.

On the basis of the module assignments of the group-level FC matrix of the healthy period at sparsity = 10%, as in previous studies,[65,69,70] we further determined the module of each node in the SCI-only group and the treatment group. We then calculated the intra-modular connectivity and inter-modular connectivity of each animal.

Hubs

Hubs play central roles by integrating and distributing information in powerful ways due to the number and position of their contacts in a network.[71] The disruptions of hub connections are related to many manifestations of brain dysfunction.[72]

The topological role of each node was determined based on its density of intra-modular and inter-modular connections by tracking the WM (Z_i) and participation coefficient (PC_i) of each node. Z_i shows how well nodes are connected within modules; it measures the number of connections of node compared with other nodes in the same module. A node with high Z_i indicates that this node is important to information exchange within the module. PC_i measures the distribution of a node's connections among the modules.[73] PC_i is close to 1 if the node is extensively linked to all other modules and zero if it is linked exclusively to nodes of its own module. A node with high PC_i indicates that this node communicates frequently with nodes in other modules.

For a node i in module c_j (j = 1, 2, …, C), Z_i and PC_i are defined as follows:

$$Z_i = \frac{k_{c_i} - \overline{k_c}}{\sigma_c}$$

$$PC_i = 1 - \sum_{c_j=1}^{C} \left(\frac{k_{c_i}}{k_i}\right)^2 x$$

where k_{c_i} is the total FC strength connected to node i in module c. $\overline{k_c}$ is defined as the mean of k_{c_i} across all nodes in module c, and σ_c is defined as the standard deviation of k_{c_i} across all nodes in module c. k_i is the total FC strength of the edges connected to node i, and C is the number of modular partitions.

Several studies have shown that hubs can be divided into provincial and connector hubs based on their topological location in the network (measured by Z_i and PC_i).[31,74,75] Connector nodes are considered to integrate information between modules for efficiency information exchange, whereas local nodes integrate information within modules for specialized function.[31,76] Local nodes are subdivided into peripheral nodes and provincial hubs that both have low PC_i, in which only provincial hubs have high Z_i (greater modular integration).[73,77]

By setting thresholds for Z_i and PC_i (thr_z and thr_{pc}), we detected hubs and divided them into provincial and connector hubs from three group-level networks. If $Z_i > thr_z$ and $PC_i > thr_{pc}$, this node was classified as a connector hub; otherwise, if $Z_i > thr_z$ but $PC_i < thr_{pc}$, it was identified as a provincial hub. In the results of this experiment, thr_z was set to 1.0 and thr_{pc} was set to 0.3. After detecting hubs of each group at each time point, we further calculated Z_i and PC_i of all ROIs of all animals in the three groups. All network analyses were performed using the Brain Connectivity Toolbox (http://www.brain-connectivity-toolbox.net)[24] and the Graph Theoretical Network Analysis (GRETNA) Toolbox in MATLAB.

Sensorimotor function evaluation

To examine the possible presence of pain, the NTPT at the healthy period, early- and late-stage postoperatively was tested and analyzed to reflect the possible pain signs post-SCI. A series of thermal stimuli generated by the laser stimulator (BWT Beijing Ltd, Beijing, CN) was applied to the skin of the animal's right (ipsilateral to the injury) hindlimb, and the stimulus intensity was recorded when the animal appears avoidance movement. The distance from the fiber port to the skin was set to 10 mm with a spot diameter ~5 mm. The current intensity ranged from 6.5 A to 11 A with a step of 0.75 A. When no obvious response to each stimulus for more than 30 s, the machine was terminated and rested for 5 min. The stimulus of each intensity is repeated three times and stopped when the animals appeared to dodge. To decrease the effect of individual variability, the stimulus intensity of each animal was divided by its own stimulus intensity in the healthy period to standardize. The ratio of the stimulation intensity post-SCI to the healthy period was used as the NTPT.

To assess the motor function, gait trajectory at the healthy period, early- and late-stages postoperatively of the right hindlimb were recorded when animals walking on the treadmill bipedally with restraining upper body. The Vicon system (Oxford Metrics Limited Company, Dayton, UK) was used to capture the step action, and the stride length was extracted for subsequent analysis. Treadmill speed was set to 0.5 m/s.

The extent of spinal cord lesions

To assess the severity of injury, the lesion area of the spinal cord at the center of the injury site was drawn manually and quantified at 1 month and 12 months post-SCI. To decrease the effect of individual variability, the lesion area at the center of the injury site of each animal was divided by its own spinal cord area in the healthy period to standardize. The ratio of the lesion area post-SCI to the SCA in the healthy period was used as the extent of SCI.

QUANTIFICATION AND STATISTICAL ANALYSIS

All statistical analyses were performed using the SPSS software version 20 (SPSS, Inc, Armonk, NY, USA). To examine the differences of FC strength, network indicators, and NTPT among the SCI-only group, the treatment group, and the healthy period, a one-way analysis of variance (ANOVA) was performed. Then, post-hoc comparisons using the LSD test (Homogeneity of variance) or Games-Howell test (Inhomogeneity of

variance) were applied. To assess the motor function and the extent of spinal cord lesions between the SCI-only and treatment groups, an independent sample t-test was executed. The nonparametric Kolmogorov-Smirnov test was performed to detect the data normality. The significance level of group differences was set at $p < 0.05$. Spearman correlation analysis was then used to study the relationships of inter- and intra-modular connectivity and injury time, and was used to study the relationship of mean FC strength between the left insula as well as bilateral somatosensory areas and the normalized thermal pain thresholds.